ACADEMIC PRESS

Available online at www.sciencedirect.com

SCIENCE DIRECT®

Journal of Sound and Vibration 263 (2003) 241–268

JOURNAL OF SOUND AND VIBRATION

www.elsevier.com/locate/jsvi

Coupled dynamics of a squeeze-film levitated mass and a vibrating piezoelectric disc: numerical analysis and experimental study

A. Minikes, I. Bucher*

Faculty of Mechanical Engineering, Technion—Israel Institute of Technology, Haifa 32000, Israel

Received 17 September 2001; accepted 4 March 2002

Abstract

This work deals with the dynamics of a vibrating piezoelectric disc, which creates, under specific vibrating conditions, an air squeeze film that is able to levitate a freely suspended object.

In such problems, the coupling effects between the various components affect the overall dynamical behaviour of the combined system. For complex systems, which combine elastic and electro-static effects together with compressible fluid effects, the coupled equations are often dealt with separately to avoid modelling and computational complexity. In this paper, the importance of handling such systems in a coupled manner is advocated by means of numerical and experimental examples. A coupled model is derived in this work making use of a concise numerical solver to allow for this investigation under several conditions. The piezoelectric part of the structure is modelled by finite elements while the squeeze film phenomenon is represented by means of finite-difference equations, to model a variant of the Reynolds equation. The numerical model was verified during each step in the development of the numerical algorithm and indeed showed good agreement with existing publications, but once the components were combined, it was found that several phenomena were misrepresented in the past due to the neglect of the coupling effects. Several physical insights are brought from the simulation and investigation of the numerical results. In the last part, the importance of coupled analysis is emphasized by introducing an experimental investigation of the dynamical behaviour while conducting a comparison with numerical simulation results. From this comparison, the limitations of state-of-the-art modelling procedures are clarified.

*Corresponding author. Tel.: +972-4-829-3153; fax: +972-4-832-4533.
E-mail address: bucher@technion.ac.il (I. Bucher).

0022-460X/03/$ - see front matter
PII: S0022-460X(02)01121-5

1. Introduction

The current tendency towards multi-disciplinary applications introduces problems with a high level of complexity. This complexity often requires an integration of several problems from different disciplines. Such integration takes place, for example, when trying to model the dynamical behaviour of a system consisting of elastic effects, electro-static effects and compressible flow effects. Integration is indeed essential because of the coupling effects that may have a significant influence on the overall behaviour. In previous papers dealing with squeeze film and air bearings that are created by the normal vibration between two vibrating surfaces (e.g., Refs. [1,2]) the analysis was carried out for the case where the mean clearance between the surfaces was pre-determined. In other words, the vibrating surface was brought (numerically) close to a fixed surface to achieve a prescribed clearance. When trying to model an applicative problem such as squeeze bearings or mass levitation, where the clearance cannot be fixed but is determined by the equilibrium of forces, the analysis appearing in the literature may prove inaccurate. Furthermore, in this case, some of the commonly used non-dimensional parameters, e.g., the squeeze number, cannot be solely used to determine the operating regime.

In addition, the dynamical analysis of vibrating piezoelectric discs, (appearing in Refs. [3,4] as well as in other references), does not incorporate the effect of interacting external loads with other components in a system. It appears that the fluid forces in a squeeze film may prove to be significant to an extent that the deformation shapes are affected.

The present paper includes two parts: numerical analysis and experimental study. The first part begins by presenting the investigated system, which was modelled and simulated, and by illustrating the numerical scheme of the solver. Later some special relations between the elastic deformations and electric fields are highlighted. The squeeze film phenomenon existing in the air layer is briefly described and finite-difference equations representing the dynamics of the fluid layer are derived. The last part of the numerical analysis presents and analyzes simulated results of the pressure distribution, the stability of equilibrium and some observations concerning the squeeze film behaviour. The second part of this paper begins by presenting the experimental system and the design considerations. Comparisons of experimental and numerical results are introduced. The response and dynamical behaviours of the floating disc are compared.

2. Numerical analysis

In this section, the equations of motion are derived part by part leading to a combined model that incorporates the fully coupled structure.

2.1. System description

Before introducing the numerical scheme of the solver and discussing the modelling considerations, the system is schematically presented.

The investigated system consists of a piezoelectric disc made of PZT-5A with polarization in the axial direction. Electrical excitation is provided by two electrodes located on the top and bottom parts of the disc and are assumed to be equi-potential. The disc is clamped at the centre of the

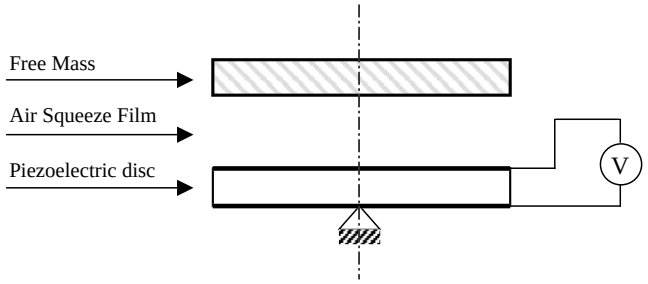

Fig. 1. Schematic layout of the system.

bottom base. A rigid mass with the same diameter as the piezoelectric disc is placed concentrically on top of the upper surface of the piezoelectric disc, while the system is surrounded by atmospheric air at standard conditions. Applying a sinusoidal voltage on the electrodes gives rise to harmonic deformation of the piezoelectric disc at the excitation frequency according to a model to be outlined in Section 2.3. At frequencies in the range of several kHz, the squeeze film phenomenon becomes significant to an extent that between the vibrating piezoelectric disc and the rigid mass, a layer of load-carrying mean pressure is created. This load-carrying air film, that is the result of normal vibratory motion between the surfaces, is able to levitate the free mass completely. Fig. 1 illustrates the schematic layout of the system.

2.2. Numerical scheme

In order to determine the overall system characteristics, the squeeze film equation together with its coupling to the piezoelectric disc and the floating disc are considered. These equations are coupled by the displacement of the floating disc relative to the vibrating piezoelectric disc and by the force exerted by the gas squeeze film on both discs. The force exerted on the floating disc changes intermittently the vertical position of the floating mass, while on the piezoelectric disc, the force exerted by the gas film gives rise to a static and dynamic deflection that influences the operating deformation shapes of the vibrating piezoelectric disc and consequently all the other state variables. Fig. 2 illustrates the numerical scheme of the solver algorithm where complete coupling is considered.

The numerical algorithm consists of three major parts. The first part derives the mass and stiffness matrices of the piezoelectric disc by means of a finite element approximation, and sets the electrical boundary conditions (the amplitude of a sinusoidal voltage). The initial conditions consist of the position and velocity of the free mass relative to the piezoelectric disc and the initial pressure distribution in the gas film. The second part of the algorithm consists of the finite-difference-based calculation of the time derivatives leading to the Reynolds equation. The Reynolds equation requires the instantaneous clearance between the discs that is obtained from vertical position of the floating disc and the deformation of the upper surface of the piezoelectric disc. The third part of the algorithm is an adaptive time integration of the dynamic equations where the coupled state-space model is integrated in time. Appendix A shows a solution for a non-linear problem in space and time using a finite-difference method in space and an adaptive integration in time.

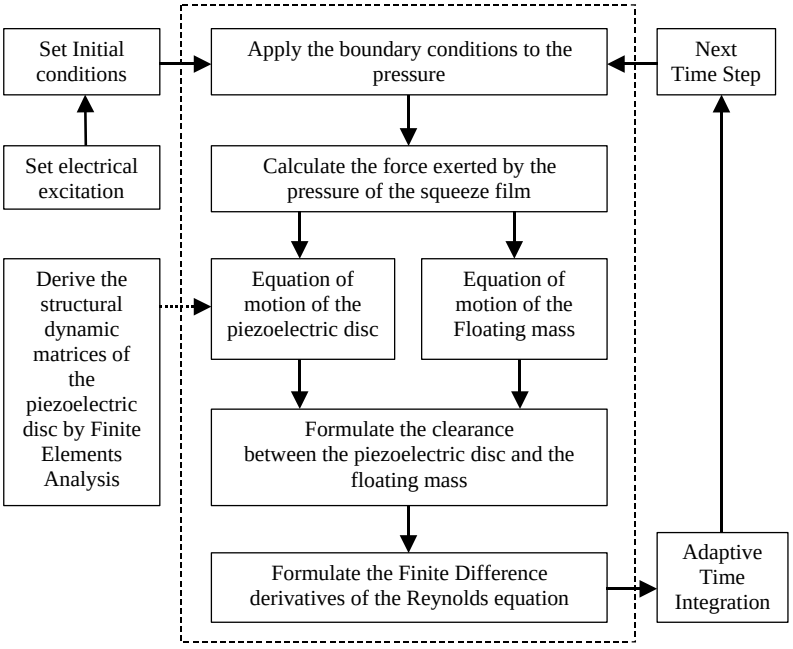

Fig. 2. Numerical scheme of the solver algorithm.

2.3. The dynamics of a piezoelectric structure

As mentioned in the description of the numerical solver, the dynamics of the piezoelectric disc are formulated by means of a finite element approximation of the piezoelectric constitutive laws.

The constitutive relations given by IEEE Std. [5] for piezoelectric media describe the coupling between the mechanical and the electrical part of the system using Einstein's summation convention:

$$T_{ij} = c^E_{ijkl} S_{kl} - e_{kij} E_k,$$

$$D_i = e_{ikl} S_{kl} + \varepsilon^S_{ik} E_k, \tag{1}$$

where T_{ij} is the mechanical stress tensor, S_{kl} is the mechanical strain tensor, D_i is the electric flux density, E_k is the electric field vector, c^E_{ijkl} is the elastic stiffness constant tensor at constant electric field, e_{ikl} is the piezoelectric constant tensor and ε^S_{ik} is the dielectric constant tensor at constant strain.

By using Hamilton's principle for non-conservative systems as done in Ref. [6], the dynamic equations of a piezoelectric structure could be directly extracted from the variational formulation. The equations of motion in matrix form can be rewritten in the so-called [H]-form [7]. This form simplifies the intermediate calculations considerably and is performed under the assumptions that the surface charge is different from zero only on the electrodes and the electric potential is set to zero on the grounded reference electrode. The matrix form of the dynamic equations may be

written as [7]

$$\begin{bmatrix} \mathbf{M}_{uu} & 0 \\ 0 & 0 \end{bmatrix} \begin{Bmatrix} \ddot{\mathbf{u}} \\ \ddot{\boldsymbol{\phi}}_p \end{Bmatrix} + \begin{bmatrix} \mathbf{H}_{uu} & \mathbf{H}_{u\phi_p} \\ \mathbf{H}^T_{u\phi_p} & \mathbf{H}_{\phi_p\phi_p} \end{bmatrix} \begin{Bmatrix} \mathbf{u} \\ \boldsymbol{\phi}_p \end{Bmatrix} = \begin{Bmatrix} \mathbf{F}_S \\ \mathbf{Q}^{(p)}_S \end{Bmatrix}, \tag{2}$$

where vector $\{\mathbf{u}\}$ is the mechanical displacement degrees of freedom (d.o.f.), vector $\{\boldsymbol{\phi}_p\}$ is the electrical potential d.o.f. on the potential electrode, $\mathbf{M}_{uu}$ is the mass matrix, $\mathbf{H}_{uu}$ is the condensed mechanical stiffness matrix, $\mathbf{H}_{u\phi_p}$ is the condensed piezoelectric coupling matrix, $\mathbf{H}_{\phi_p\phi_p}$ is the condensed dielectric stiffness matrix, $\mathbf{F}_S$ is the surface traction and $\mathbf{Q}^{(p)}_S$ is the surface electric charge on the potential electrode.

Under a harmonic excitation voltage $\boldsymbol{\phi}_p = \boldsymbol{\phi}_0 \sin(\omega t)$ and in the absence of electrical inertia, the equations of motion can be written as

$$[\mathbf{H}_{uu} - \omega^2 \mathbf{M}_{uu}]\{\mathbf{u}_0\} = \{\mathbf{F}_0\} - [\mathbf{H}_{u\varphi}]\{\boldsymbol{\phi}_0\}. \tag{3}$$

Eq. (3), contains a static reduction of the electric d.o.f., and is thus of a dimension compatible with the mechanical d.o.f.

The eigenvalue problem of the piezoelectric structure is calculated for the case when there are no external excitations on the structure, which means in the present case that there are no surface tractions and no potential voltage on the electrodes. This case is equivalent to a short-circuit case.

Therefore with $\mathbf{F}_0 = \mathbf{0}$ and $\boldsymbol{\phi}_0 = \mathbf{0}$ the eigenvalue problem takes the form:

$$[\mathbf{H}_{uu}][\boldsymbol{\Psi}] = [\mathbf{M}_{uu}][\boldsymbol{\Psi}][\boldsymbol{\Omega}^2], \tag{4}$$

where $[\boldsymbol{\Omega}^2]$ contains the eigenvalues on its diagonal and $[\boldsymbol{\Psi}]$ is the eigenvectors matrix.

The system dealt with here is axisymmetric; therefore a two-dimensional element was chosen for the finite elements analysis. The piezoelectric disc was modelled by a four-node plane element having three d.o.f. at each node: electric potential, radial displacement and axial displacement. Isoparametric bilinear interpolation functions and Gauss quadrature integration have been used.

In order to verify the correctness of the finite element model that was developed, a comparison with the numerical results obtained by Gou et al. [3] was made and the results are presented in Appendix B.

2.3.1. *Special relations between the elastic and electric effects*

Examination of the mode shapes of the piezoelectric disc, reveals that for extensional mechanical mode shapes (symmetrical around the *r*-axis in Fig. 3), the electric field in the disc's cross section is anti-symmetric around the *r*-axis as can be seen in Fig. 3(b), while for flexural mechanical mode shapes, the electric field in the disc's cross-section is symmetric around the *r*-axis as seen in Fig. 3(a). Indeed, it was mentioned by Gou et al. [3] that only extensional modes could be excited electrically by a voltage applied across electrodes on the top and bottom surfaces of the disc. The electric field distribution, as was described above, provides an explanation to this fact as a symmetrical electric field distribution around the *r*-axis means that there is no potential gradient between the top and bottom surfaces of the disk and thus the flexural modes are completely decoupled from the applied voltage across the electrodes.

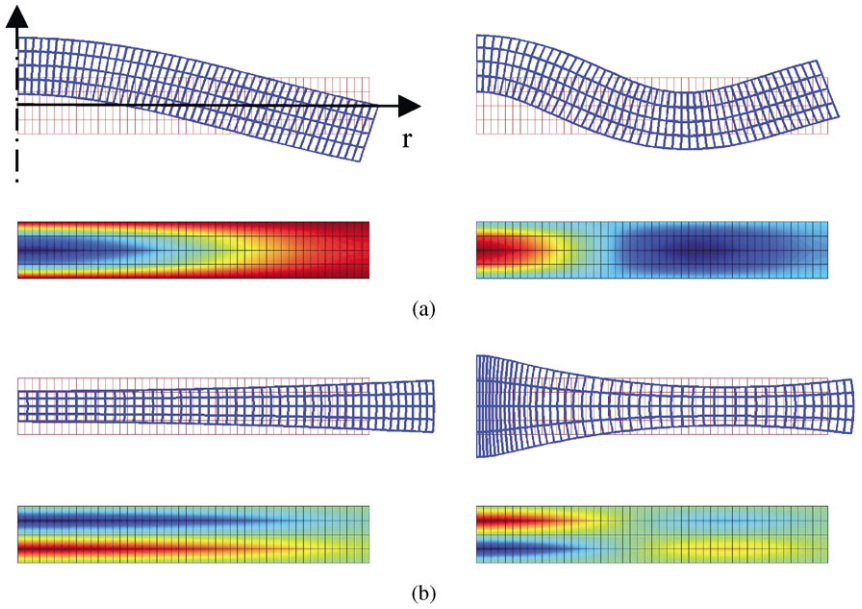

Fig. 3. (a) Two examples of flexural mechanical modes and symmetrical electric potential field along the radial axis; (b) two examples of extensional mechanical modes and the anti-symmetrical electric potential field along the radial axis.

2.3.2. *Frequency response functions*

Assuming that a harmonically varying voltage at a frequency ω excites the piezoelectric element, the components of the mechanical displacement may then be calculated by the mode superposition method [3]. By introducing the transformation $\{\mathbf{u}_0\} = [\tilde{\boldsymbol{\psi}}]\{\mathbf{z}_0\}$ into Eq. (3) and pre-multiplying by $[\tilde{\boldsymbol{\psi}}]^{\mathrm{T}}$, where $[\tilde{\boldsymbol{\psi}}]$ is the mass-normalized modal matrix, the frequency response function can be expressed by

$$\{\mathbf{u}(t)\} = \{\mathbf{u}_0\}\mathrm{e}^{\mathrm{j}\omega t} = \sum_{r=1}^{N} \frac{\{\tilde{\boldsymbol{\psi}}\}_r \{\tilde{\boldsymbol{\psi}}\}_r^{\mathrm{T}} (\{\mathbf{F}_0\} - [\mathbf{H}_{u\varphi}]\{\boldsymbol{\phi}_0\})}{(\omega_r^2 + \mathrm{j}\eta_r\omega_r^2 - \omega^2)} \mathrm{e}^{\mathrm{j}\omega t}, \tag{5}$$

where $\{\mathbf{z}_0\}$ is a vector of modal displacements, $\{\tilde{\boldsymbol{\psi}}\}_r$ is the eigenvector related to mode r, and η_r, ω_r are the damping loss and the structure's natural frequency for mode r, respectively. Numerical results showing the frequency response of a piezoelectric disc are presented in Appendix B.

2.4. *The squeeze film effect*

An oscillating motion in the normal direction between parallel surfaces can generate an air film with a mean pressure higher than the surrounding. This load-carrying phenomenon arises from the fact that a viscous flow cannot be instantaneously squeezed, therefore providing a cushioning effect and the film equilibrium is established though a balance between viscous flow forces and compressibility forces.

The squeeze film effect occurs, for standard air, when the oscillations are at high frequencies (in the kHz range) with sub-millimetre amplitudes. Under these conditions, the viscous forces (flow

resistance) will be high enough to introduce compressibility effects, i.e., the flow will be compressed and expanded periodically.

Reynolds equation is the differential equation governing the pressure distribution in the squeeze film. This equation can be derived from the Navier–Stokes equation and the continuity equation under the following assumptions: (1) Newtonian flow and air acts as an ideal gas, (2) laminar and isothermal flow, (3) smooth surfaces, (4) the gas film thickness is much smaller than the bearing dimensions so that the velocity gradients in the radial and tangential direction are negligible compared with the velocity gradients in the normal direction.

When fluid inertia and dilatational stresses in the fluid are negligible, the pressure in a thin, isothermal gas film is governed by a non-linear partial differential equation commonly addressed as Reynolds equation [8]:

$$\frac{\partial}{\partial x_i}\left(h^3 p \frac{\partial p}{\partial x_i}\right) = 6\mu\left\{2\frac{\partial (ph)}{\partial t} + \frac{\partial}{\partial x_i}\left[ph(V_i - V_i')\right]\right\}, \tag{6}$$

where h is the film thickness, p is the fluid pressure, μ is the fluid viscosity and V_i, V_i' are the velocities of the surfaces in the x_i direction.

By introducing the non-dimensional parameters

$$P = \frac{p}{p_a}, \quad R = \frac{r}{r_0}, \quad H = \frac{h}{h_0}, \quad T = \omega t, \tag{7}$$

the normalized Reynolds equation in polar co-ordinates for an ideal gas, flowing between two parallel circular discs becomes

$$\frac{1}{R}\frac{\partial}{\partial R}\left(PRH^3 \frac{\partial P}{\partial R}\right) = \sigma \frac{\partial (PH)}{\partial T}, \tag{8}$$

where the squeeze number σ is defined as

$$\sigma = \frac{12\mu\omega r_0^2}{p_a h_0^2} \tag{9}$$

and ω is the squeeze motion vibration frequency; p_a is the atmospheric pressure, r_0 is the disc radius and h_0 is the initial clearance between discs.

The pressure at the disc edge is the atmospheric pressure and because of symmetry, there is no pressure gradient at the disc's centre. Therefore the boundary conditions are

$$P(R = 1, T) = 1, \quad \frac{\partial P}{\partial R}(R = 0, T) = 0. \tag{10}$$

In the initial state, the pressure between the discs is atmospheric:

$$P(R, T = 0) = 1. \tag{11}$$

The total film force exerted on the disc as function of time is given by

$$W(T) = \frac{f_t}{p_a r_0^2} = 2\pi \int_0^1 R(P - 1)\,\mathrm{d}R. \tag{12}$$

By application of a finite-difference scheme in space, the Reynolds equation takes the form of a set of ordinary normalized differential equations in time:

$$\sigma\left(\frac{\partial P}{\partial T}\right) = -\frac{P_i}{H_i}\left(\frac{\partial H}{\partial T}\right)_i + \frac{P_i H_i^2}{R}\left(\frac{\partial P}{\partial R}\right)_i + H_i^2\left(\frac{\partial P}{\partial R}\right)_i^2 + 3P_i H_i\left(\frac{\partial P}{\partial R}\right)_i\left(\frac{\partial H}{\partial R}\right)_i + P_i H_i^2\left(\frac{\partial^2 P}{\partial R^2}\right)_i, \tag{13}$$

where $H = H(R, T)$ is the clearance between the discs as a function of radial co-ordinate and time. The boundary conditions for the finite-difference scheme are given by Eq. (10).

2.5. Formulating the coupled dynamics

The equations of motion of the system, with consideration of the coupling effects, can be described by a state-space formulation as shown below.

As the floating mass is assumed rigid, the motion of the floating disc in the axial direction can be described by one d.o.f. (designated by X). The normalized equation of motion of the floating disk can be written as

$$\frac{\partial^2 X}{\partial T^2} = \ddot{X} = F - G. \tag{14}$$

With the non-dimensional parameters

$$X = \frac{x}{h_0}, \quad F = \frac{f_t}{m h_0 \omega^2}, \quad G = \frac{g}{\omega^2 h_0}, \quad T = \omega t,$$

where h_0 is the initial clearance between discs, m represents the mass of the floating disk, ω is the excitation frequency, f_t is the total force exerted by the squeeze film on the disc (taken from Eq. (12)), and g stands for acceleration due to gravity.

In order to express the equation of motion of the piezoelectric disc in state space, Eq. (3) is written in the time domain as

$$[\mathbf{M}_{uu}]\{\ddot{\mathbf{u}}\} + [\mathbf{C}_{uu}]\{\dot{\mathbf{u}}\} + [\mathbf{H}_{uu}]\{\mathbf{u}\} = \{\mathbf{f}\} - [\mathbf{H}_{u\varphi}]\{\boldsymbol{\phi}\}. \tag{15}$$

The damping matrix added to the equation is defined as $[\mathbf{C}_{uu}] = \left[\tilde{\boldsymbol{\psi}}\right]^{-\mathrm{T}}[2\xi\omega_r]\left[\tilde{\boldsymbol{\psi}}\right]^{-1}$ in the physical co-ordinates or a diagonal matrix $[2\xi\omega_r]$ in modal co-ordinates. The motivation for such formulation is clarified below. In this study, a damping factor of $\xi = 0.01$ was used.

As the thickness of the squeeze film is much smaller compared to the radius of the discs, the pressure gradient in the axial direction is negligible, allowing one to describe the pressure distribution in the radial direction by a one-dimensional grid in a finite-difference model. In order to simplify the meshing procedure, the fluid grid is chosen to be identical to the grid of the upper nodal points of the piezoelectric disc's cross-section.

The distributed pressure gives rise to a force vector $\{\mathbf{f}\}$ exerted by the air film on the piezoelectric disc. These equivalent forces are applied to the nodes of the upper surface of the piezoelectric disc and their compressive effect can be approximated by

$$\{\mathbf{f}\}_i = -2\pi P_a r_0^2(\mathbf{R}_i(\mathbf{P}_i - 1)\Delta\mathbf{R}), \quad \Delta\mathbf{R} = \mathbf{R}_{i+1} - \mathbf{R}_i. \tag{16}$$

In order to achieve better numerical accuracy of the solution, it is essential to normalize the equations of motion, therefore as Eqs. (13) and (14) are already normalized, a similar procedure is applied to Eq. (15) as well. By introducing the transformation $\{\mathbf{u}\} = [\tilde{\boldsymbol{\psi}}]\{\mathbf{z}\}$ into Eq. (15) and pre-multiplying by $[\tilde{\boldsymbol{\psi}}]^{\mathrm{T}}$, where $[\tilde{\boldsymbol{\psi}}]$ is the mass-normalized modal matrix, Eq. (15) can be expressed by

$$[\mathbf{I}]\{\ddot{\mathbf{Z}}\} + 2\xi[\boldsymbol{\Omega}_r]\{\dot{\mathbf{Z}}\} + [\boldsymbol{\Omega}_r^2]\{\mathbf{Z}\} = \{\mathbf{F}_t\} - \{\mathbf{F}_\phi\}, \tag{17}$$

where $\{\mathbf{z}\}$ is a vector of generalized co-ordinates, $[\boldsymbol{\Omega}_r^2]$ is a matrix having the undamped eigenvalues on its diagonal, and the non-dimensional parameters of this equation are

$$\{\mathbf{Z}\} = \frac{\{\mathbf{z}\}}{h_0}, \quad \{\mathbf{F}_t\} = \frac{[\tilde{\boldsymbol{\psi}}]^{\mathrm{T}}\{\mathbf{f}\}}{h_0\omega^2}, \quad \{\mathbf{F}_\phi\} = \frac{[\tilde{\boldsymbol{\psi}}]^{\mathrm{T}}[\mathbf{H}_{u\varphi}]\{\boldsymbol{\phi}\}}{\omega^2 h_0}.$$

By defining the state-space variables vector $\mathbf{q} = \{X\ \dot{X}\ \mathbf{P}\ \mathbf{Z}\ \dot{\mathbf{Z}}\}^{\mathrm{T}}$, where $X, \dot{X}$ are scalars representing the position and velocity of the floating disc, respectively, $\mathbf{P}$ is the pressure vector in the squeeze film along the radial axis, and $\mathbf{Z}, \dot{\mathbf{Z}}$ are the modal displacements and velocities vectors of the nodes of piezoelectric disc, respectively. The state-space formulation takes the form:

$$\begin{Bmatrix} \dot{X} \\ \ddot{X} \\ \dot{\mathbf{P}} \\ \dot{\mathbf{Z}} \\ \ddot{\mathbf{Z}} \end{Bmatrix} = \begin{bmatrix} 0 & 1 & 0 & 0 & 0 \\ 0 & 0 & 1 & 0 & 0 \\ & \text{Eq. (13)} & & & \\ 0 & 0 & 0 & 0 & [\mathbf{I}] \\ 0 & 0 & 0 & -[\boldsymbol{\Omega}_r^2] & -2\xi[\boldsymbol{\Omega}_r] \end{bmatrix} \begin{Bmatrix} X \\ \dot{X} \\ \mathbf{P} \\ \mathbf{Z} \\ \dot{\mathbf{Z}} \end{Bmatrix} + \begin{Bmatrix} 0 \\ \mathbf{F} - \mathbf{G} \\ \mathbf{0} \\ \mathbf{0} \\ \mathbf{F}_t - \mathbf{F}_\phi \end{Bmatrix}. \tag{18}$$

The electrical force $\{\mathbf{F}_\phi\}$, resulting from the induced voltage on the electrodes, obtains its final form by inserting $\boldsymbol{\phi} = \boldsymbol{\phi}_0 \sin(\omega t)$ into Eq. (18). The non-linear coupling takes place within F_t where the effect of pressure variation that depends on the mechanical displacement plays an important role. Eq. (18) shows that the coupling of the system's component equations, takes place in the applied forces ($\mathbf{F}$ and $\mathbf{F}_t$) and in the finite-difference expressions represented by Eq. (13). As explained earlier, the definition of the gap between the discs $\mathbf{H} = \mathbf{H}(\mathbf{R}, \mathbf{T})$ in Eq. (13) is determined by the displacements of the freely floating mass, and the position of the upper surface of the piezoelectric disc.

2.6. Simulations results

In practice, the deformations of one thick piezoelectric disc are not sufficient, in terms of amplitude of vibration, to produce the conditions that will create a squeeze film with a sufficient load-carrying capacity. In order to obtain larger vibration amplitudes, a useful design that increases the vibration amplitudes to a sufficient amount is discussed later on in this work in the experimental study. For the sake of simplicity at this stage, an impractically large voltage is numerically applied to the electrodes in the range of several kV and the behaviour of the piezoelectric material is still considered to be linear.

The piezoelectric disc's model is divided into a (5×25) nodal points (4×24 elements); and the pressure finite-difference scheme makes use of the same nodal points in the radial direction thus creating a grid of 25 points. This mesh provided the necessary accuracy for the excited wavelengths.

The physical parameters of the system under which the numerical simulation was carried out are summarized in Table 1.

2.6.1. Pressure distribution

Examination of the influence of the boundaries on the flow cycle indicates that, during the compression stage, the increase in pressure causes outward flow, but at the same time, the clearance decreases, allowing only little airflow to occur. On the other hand, during the decompression stage, while the pressure drops, the flow changes its direction becoming an inward flow. At this stage, the clearance between the discs increases, allowing a larger flow rate to enter at a relatively slow velocity.

The numerical algorithm enables one to calculate the pressure distribution between the discs for a given radius as a function of time. Observing the normalized pressure distribution, as shown in Fig. 4, reveals that near the edges of the disc, the mean pressure does not exceed the value 1.0 (i.e.,

Table 1
The physical parameters under which the numerical simulation was carried out

Parameters of the system		Parameters of the interfering force applied on the mass	
Piezoelectric disc diameter	40 mm	Applied force	3 N
Piezoelectric disc thickness	10 mm	Initial time	33.7 ms
Excitation voltage	10 kV	Duration	3.7 ms
Excitation frequency	8700 Hz		
Floating mass	0.1 kg		
Initial clearance	100 μm		

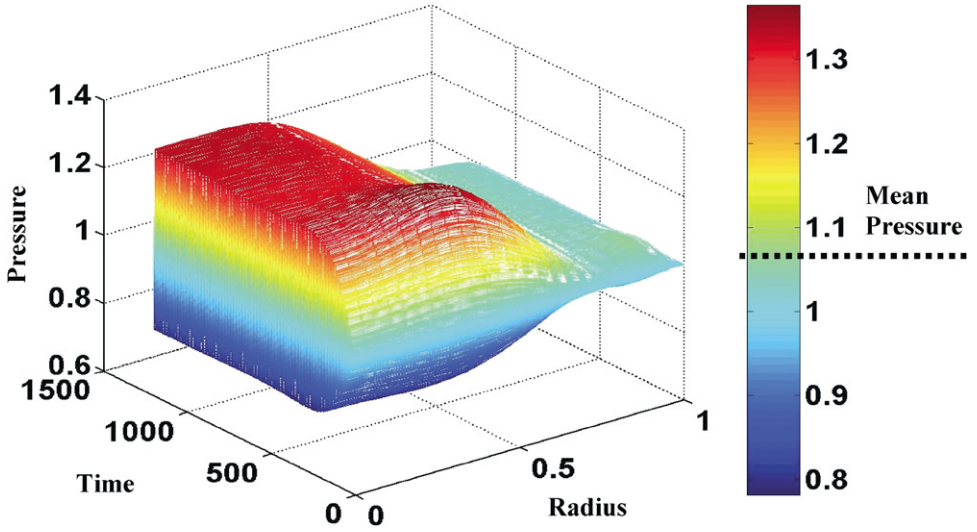

Fig. 4. Pressure distribution (normalized by atmospheric pressure) between the discs as a function of the radial location and time.

normalized atmospheric pressure). Furthermore, the fluid near the edges barely experiences any compression or decompression; therefore no cushioning effect takes place in this region. As can be seen in Fig. 4, the squeeze film phenomenon takes place close to the centre of the discs, where the pressure cycle is changing from compression to decompression while the mean pressure is above the atmospheric pressure.

2.6.2. System's equilibrium stability

In order to examine, the dynamical behaviour of the system (Fig. 1) after reaching steady state equilibrium, an interfering force is numerically applied to the free mass for a short period of time. The force was applied downward, pushing the free mass towards the vibrating piezoelectric disc. The physical parameters of the interfering force, under which the numerical simulation was carried out, are summarized in Table 1.

Fig. 5(a) shows the clearance between the discs as a function of time. It is seen that under the conditions given in Table 1, after approximately 30 ms, the system reaches equilibrium where the mean clearance is near 70 μm. At this point in time, an external force of 3 N was applied to the floating disc for a period of 3.7 ms. There is an immediate decrease in the gap, which remains smaller, as long as the floating disc is subjected to the force. When the interfering force is terminated, the floating mass returns to the prior gap of equilibrium, which indicates that this equilibrium is indeed stable. Fig. 5(b) shows the change in the force exerted by the squeeze film (Eq. (12)) on the surfaces as a function of time. It is clearly seen that when the interfering force is applied downwards on the floating disc, the force exerted by the squeeze film increases, resisting the interfering force. The mean force exerted by the squeeze film when no interfering force exists is equal to the gravitational force of the floating disc.

2.6.3. Case of a fixed upper mass

In previous papers dealing with squeeze film air bearing created by normal vibration between two surfaces [1], the analysis treated the case where the mean clearance between the surfaces was predetermined. In other words, the vibrating surface was brought close to a fixed surface to a required clearance. In the case of the floating mass, this assumption obviously does not generally apply.

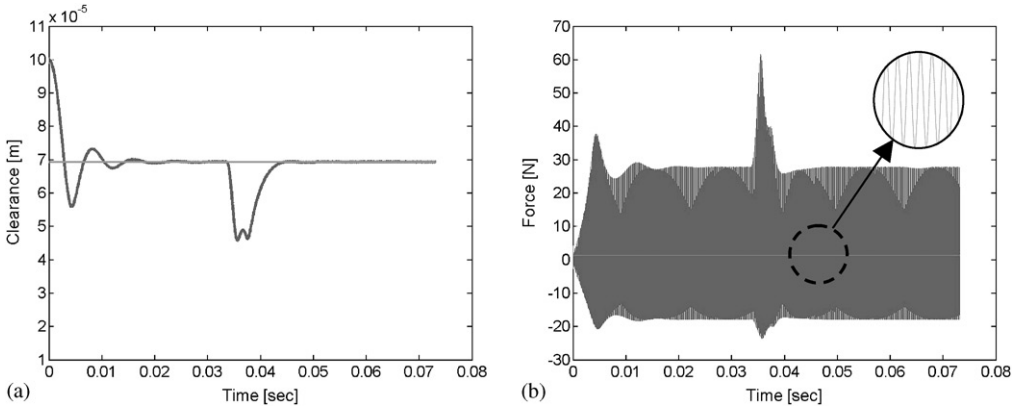

Fig. 5. Numerical simulation of the system behaviour under an interfering force applied downward on the floating disc: (a) the clearance as a function of time; (b) the force exerted by the squeeze film as a function of time.

When examining the behaviour of the air film undergoing periodic cycles of compression and decompression, with the assumption of prescribed mean clearance between the surfaces, one can observe that at relatively low frequencies or relatively large gaps (small squeeze number σ), the force exerted by the film, Eq. (12), is proportional to the squeeze velocity, which means that the film acts as a viscous damper. While, at relatively high frequencies or relatively small gaps (large squeeze number σ), the force exerted by the film is proportional to the squeeze clearance rather than the squeeze velocity. For such conditions, the film becomes virtually non-dissipative, showing a non-linear spring action. In practice, the film represents a combination of "viscous damping" and "spring" actions [1].

Fig. 6 shows numerical results (normalized) of the force exerted by the film and the periodic cycle of the clearance for a case where the floating mass is clamped, allowing one determine the mean clearance. Case (a) shows numerical results under conditions where the squeeze number σ is small. It is seen that, the phase between the force and the clearance is nearly $\pi/2$ which indicates that the force is proportional to the squeeze velocity. Case (b) shows numerical results for which the squeeze number σ is large. It is seen that in this case, the phase between the force and the clearance is nearly zero, which indicates that the force is proportional the squeeze clearance.

2.6.4. *Case of a freely floating upper mass*

When the mass is free to float with no constraints, the mean clearance cannot be prescribed as was done in the former case. The mean gap is determined by the dynamics of the system with the coupling effects involved. It turns out that in such case, the squeeze number σ is no longer a physical indicator for the squeeze-film's behaviour.

An examination of the behaviour of the air film for the case of a floating mass reveals that the behaviour is no longer the same as was for the case of prescribed mean gap. Figs. 7(a) and (b) show the phase between the force exerted by the squeeze film and the displacement of different points on the vibrating surface as a function of the excitation frequency. It can be noticed that in much of the excitation frequency range, the phase between the force exerted by the squeeze film and the displacement of the vibrating surface (in our case, points on the upper surface of the piezoelectric disc), is ether $\pm 180^\circ$ or zero. This behaviour indicates that at these frequencies, the squeeze film acts as a non-linear spring without a dissipative mechanism. Fig. 7(c) shows the clearance between the discs as function of the excitation frequency. We can observe that the

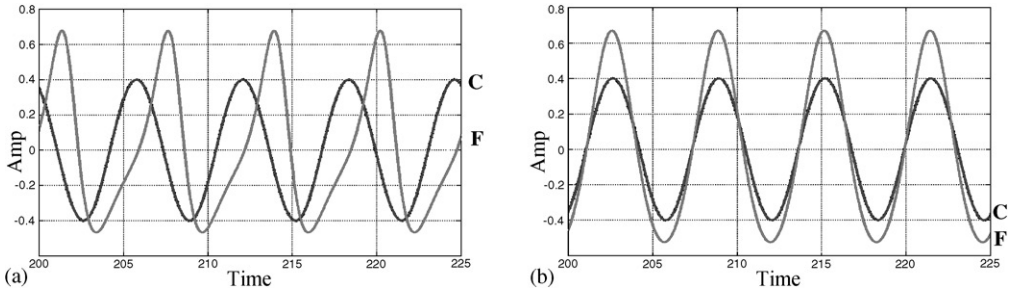

Fig. 6. Numerical results (normalized) of the force (F) exerted by the film and the periodic variation of the clearance (C) for a case where the upper mass is fixed in space: (a) small squeeze number: $\sigma = 10$; (b) large squeeze number: $\sigma = 1000$.

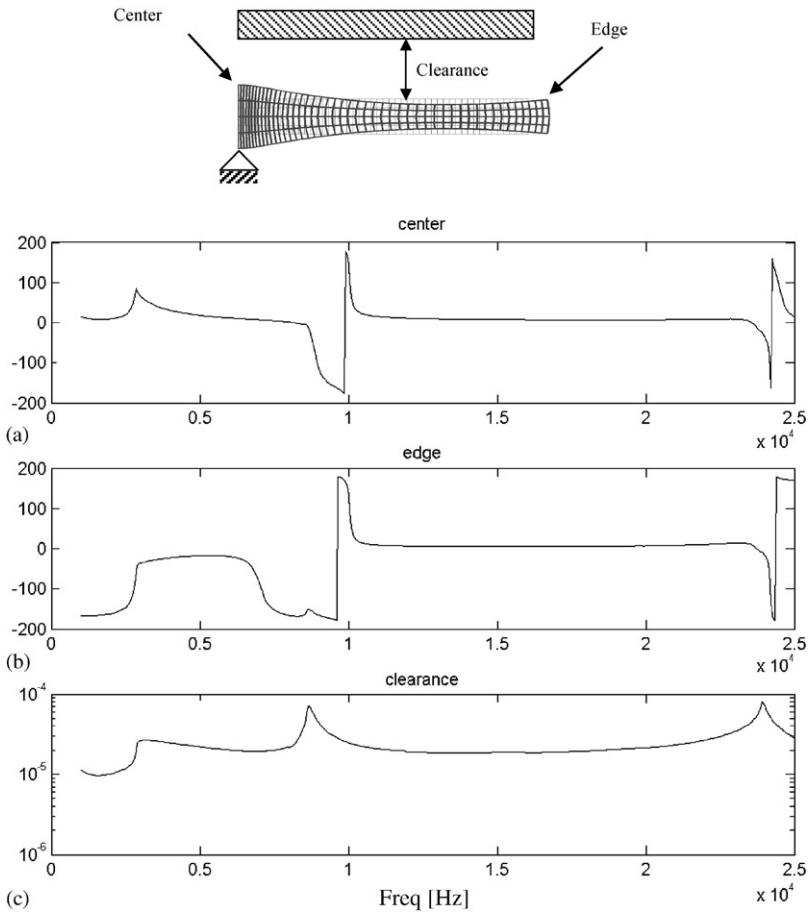

Fig. 7. The phase between the force exerted by the squeeze film and the displacement of (a) the centre point and (b) the edge point on the vibrating surface as a function of the excitation frequency; (c) the absolute value [m] of the clearance between the discs as a function of frequency.

changes in the phase (Figs. 7(a) and (b)) occur near the resonance frequencies of the complete system (3500, 8800, 23,500 Hz) where the clearance increases. Furthermore, as expected, the differences in synchronization between the phases for the different points on the vibrating surface are related to the piezoelectric mode shapes. This can be easily seen near the first resonance frequency (3500 Hz) where the edge point is in anti-phase to the centre point as should be according to corresponding mode shape. It is interesting to note that the transition to a damper-like behaviour starts at regions where the amplification is largest (resonance).

The former conclusions about the behaviour of the system for the case where the mass is free to float are insufficient. When plotting the clearance between the discs as function of time for different initial gaps, one sees that at any chosen excitation frequency, the mass displacement relative to the piezoelectric disc is strongly damped, reaching the equilibrium gap with almost no overshot. While reaching this equilibrium, the mass keeps vibrating at the excitation frequency

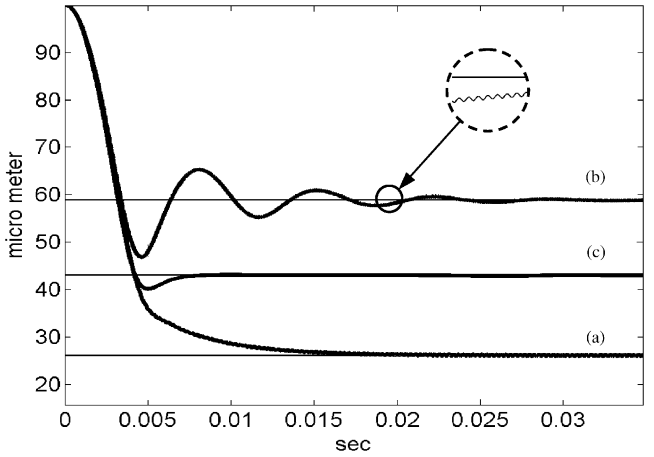

Fig. 8. Numerical simulation of the clearance vs. time for three different excitation frequencies: (a) 3500 Hz, (b) 8800 Hz, (c) 23500 Hz.

with small amplitudes relative to the clearance. Fig. 8 shows numerical simulation of the clearance versus time as the system is electrically excited at the first three resonant frequencies. In all simulations, the floating mass vibrates, has a superimposed fine motion at the excitation frequency (see enlargement in Fig. 8). Such behaviour may suggest that the squeeze film acts as a non-linear spring (this is expected due to the compressibility effects of air and from the mathematical representation by Reynolds's equation).

To summarize the analysis of the numerical results, it can stated that: (1) the non-linear spring action of the squeeze film is related to the variations in the clearance between the discs. (2) When large variations in the clearance take place, the stiffness of the squeeze film is relatively low, allowing for the damping mechanism of the viscous flow to become dominant, while (3) at relatively small clearance variations, the stiffness of the squeeze film increases dramatically, consequently making the squeeze damping insignificant. (4) The damping factor decreases as the mean clearance increases.

3. Experiments, design and comparison

In this section, the importance of coupled analysis is emphasized by introducing an experimental investigation of the dynamical behaviour while conducting a comparison with the numerical simulation results. From this comparison, the limitations of state-of-the-art modelling procedures are clarified. There have been several design considerations in the construction of the experimental model concerning the layout of a piezoelectric stack of discs and an exponential horn for amplifying the system's vibrations. These design enhancements allowed the squeeze film phenomenon to take place and carry a reasonable load during the laboratory measurements. The comparison of the simulated results with the measurements shed more light on the true physical behaviour of the device.

3.1. Description of the experimental and measurement system

This numerical model shown in Fig. 1 is oversimplified when trying to design a working system according to commonly used lumped parameter models. As the piezoelectric material could withstand a limited voltage, the deformations in the piezoelectric disc are insufficient to produce an air squeeze film. Reducing the disc's thickness dramatically or clamping the disc close to its nodal diameter, does not provide a sufficient solution as new problems arise such as static deflections and manufacturing difficulties.

The modified system consists of four piezoelectric discs arranged in a stack formation with electrodes between them and opposite polarization in the thickness direction. The stack is clamped to a large base at the bottom end and on the top base an exponential horn, made of steel, is attached. To the small diameter of the horn, a thin disc made of aluminium was attached. These modifications, which are deigned to increase the vibration amplitudes of the aluminium disc, are discussed later. Fig. 9 illustrates the schematic layout and a photograph of the experimental system. The dimensions and materials of the system are detailed in Table 2.

3.1.1. Experimental system design considerations

When designing a piezoelectric transducer, it is desirable to achieve the largest possible displacements. Therefore, the transducer is composed of discs arranged in a concentric stack with electrodes between the discs. As in a parallel plate capacitor, in such an assembly, the electric field on each disc is stronger in comparison to a single disc having a thickness equal to the total stack thickness.

As long as the applied voltage is in the linear range of the piezoelectric material, the deformations are proportional to the applied voltage. Therefore by arranging the polarity of the

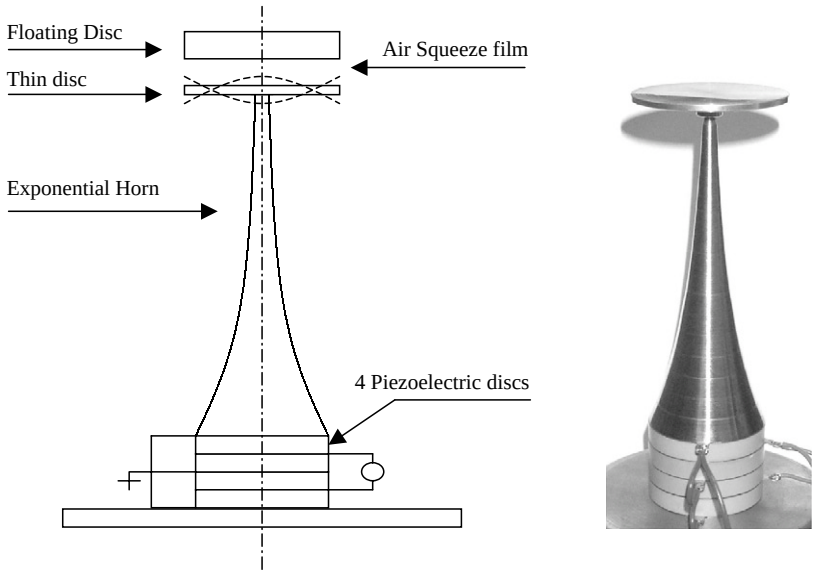

Fig. 9. Schematic layout and a photograph of the experimental system.

Table 2
The dimensions and materials of the system

Component	A. Material	Parameter	Dimension (mm)
Piezoelectric discs	PZT-5A	Diameter thickness	50 10
Electrodes	Copper	Diameter Thickness	50 1
Exponential horn	Steel	Large diameter Small diameter Length	50 5 160
Thin disc	Aluminium	Diameter Thickness	60 3
Floating disc	Aluminium	Diameter	60

discs intermittently in opposite directions, the deformations accumulate, producing larger relative displacements between the tips of the stack.

When a piezoelectric transducer is excited by electrical voltage, there are limitations on the amount of obtainable mechanical power. The voltage amplifier limits the mechanical power that can be obtained, and so does the breakdown voltage of the piezoelectric medium. A third factor is the temperature rise that the piezoelectric medium can withstand without changing its properties.

Under vibrating conditions, a mechanical amplifier shaped as a horn (see Fig. 9) and connected to the piezoelectric stack can increase the strain or the motion to a sufficient amount. The horn is in effect a half-wave transformer that tapers from a large diameter on the transducer end to a small diameter on the load end [9]. This transformer increases the local velocity by the ratio of the large diameter to the small diameter of the transforming horn.

In order to verify and compare the experimental results to the numerical ones, the numerical model must be modified so that the dynamical behaviour of the complex piezoelectric actuator could be simulated. Therefore, the finite element model was modified to be able to combine the various components of the actuator. A useful and convenient way to model a complex system is by sub-dividing the system into a group of smaller and simpler problems, solving each problem separately and then regrouping the system's components under the appropriate constrains. Such an approach is made possible by a transformation, which allows only motions that do not perform any work on the immovable constraints (see Appendix C). In this work, this transformation was performed in order to combine the stack of piezoelectric discs together with the exponential horn and the thin disc.

3.1.2. The measurement system

The configuration of the measurement system consisted of a laser sensor allowing one to measure displacements and velocities normal to the laser beam. Two mirrors providing two d.o.f.

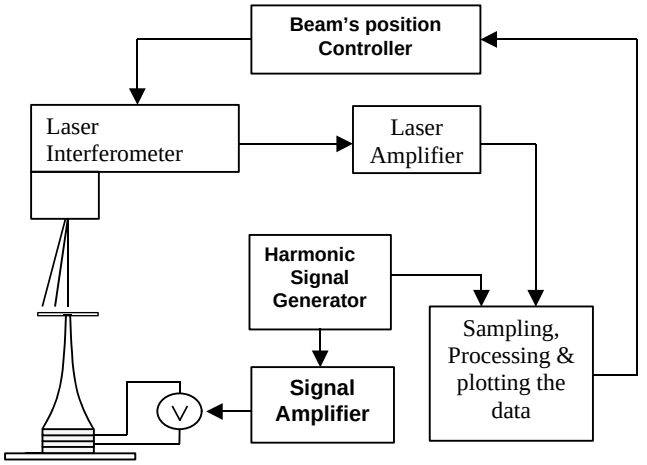

Fig. 10. Schematic layout of the measurement equipment.

control the beam's position, allowing one to scan flat surfaces. Fig. 10 shows a schematic layout of the measurement equipment. The frequency response functions were found by curve fitting the laser's measurement signals. Measuring points on the thin disc according to a polar grid and plotting the displacement amplitude of each co-ordinate synchronized with its relative phase produce the operating mode shapes (as shown later in Section 3.2.2).

3.2. Comparison of experimental and numerical results

In this section, the dynamical behaviour of the numerical model and the experimental system are compared under various excitation patterns.

3.2.1. Frequency response function

At this stage, the system components that are: the piezoelectric stack, the exponential horn and the thin disc, are all connected with the relevant constraints. The first step before examining the system's dynamics is to verify the numerical algorithm by comparing the simulated results to measured results. Fig. 11 shows the amplitude of the displacement at the centre point on the upper surface of the thin disc as a function of frequency. This figure includes the numerical results calculated by the finite elements model together with the measurement results. In addition, a plot of the numerical results done by commercial software—Ansys5.6, is superimposed.

As seen from Fig. 11, a relatively good agreement was achieved. The difference in the results is due to several possible causes. In the numerical model, an assumption of perfect and aligned connection of the system's components was made. In practice, due to design constraints, such ideal connections are not obtained. Therefore in the experimental model, the stack consists of discs with a small hole in the centre through which a screw passes to fasten together the stack and the horn. Such constraints cause variation in the stiffness and damping of the system and render the assembly to be slightly asymmetric.

3.2.2. Mode shapes

A natural step towards verifying the numerical results was taken by measuring the mode shapes of the system and comparing them with the mode shapes that were obtained by the numerical simulation.

The measurements of the mode shape were performed by measuring points on the thin disc according to a polar grid with a division of 8 circles and 30 sections starting at an initial radius. The mode shapes are found by plotting the displacement amplitude of each co-ordinate on the polar grid synchronized with its phase. Fig. 12 shows the plots of the measured data and the corresponding plots of the numerical results. One can see that the finite element analysis predicts nearly identical mode shapes to the measured ones. The computed plots in Fig. 12 show only a part of the model, which mostly influence the squeeze film. But the numerical model incorporates the prediction of the entire structure described in Fig. 9.

3.2.3. The dynamics of the floating mass

In this section, the focus is on the dynamics of the floating mass and in particular, comparison between the transient behaviour and the steady state gap under several loading conditions.

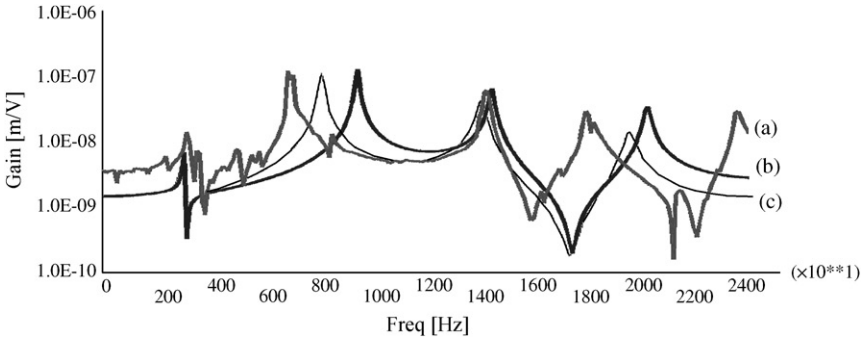

Fig. 11. The frequency response function of the displacement of centre point on the upper surface of the thin disc: (a) measurement; (b) finite element model; (c) Ansys 5.6.

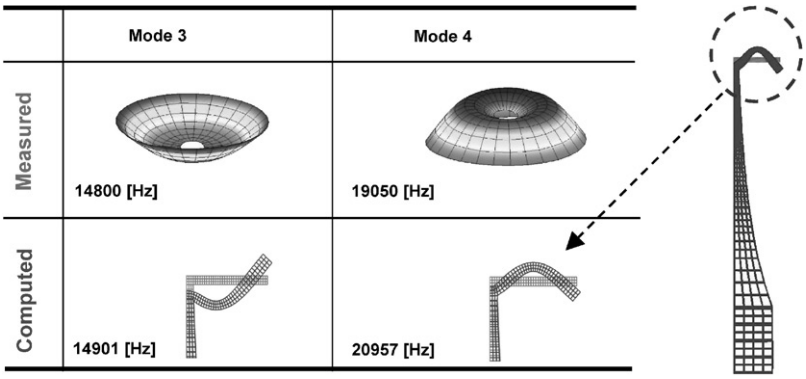

Fig. 12. Measured and numerical results of two mode shapes of the thin disc connected to the horn's tip.

3.2.3.1. Mean clearance at equilibrium—a comparison. The most valuable part of the experiments consists of measuring the dynamical behaviour of the floating mass. In this part of the measurements, the laser sensor beam was located above and normal to floating mass (see Fig. 10), allowing one to measure displacements and velocities of the floating mass. Waiting a sufficient amount of time, the squeeze film reaches a steady-state equilibrium in the axial direction, but in the radial direction the equilibrium is unstable, so that any minor asymmetric imperfection in the model causes the mass to slip sideways. To prevent the sideways motion, a thin cotton cord was stretched parallel to the disc's surface, connecting the centre of the mass to a fixed support. The cord's weight is negligible in comparison to the weight of the floating disc and by such a set-up, the cord applies tension force only in the radial direction without applying any moment. Once the mass was floated, the direction of the cord's pulling force was set opposite to the sliding direction, preventing it from slipping sideway. In this way, one could keep the floating disc in a concentric line with the transducer with minimal interference.

A measurement of the mean clearance between the transducer and the floating mass once the system achieved equilibrium was performed. The mean clearance steady state was found by measuring the displacement of the floating disc while turning the excitation voltage off. Figs. 13(a) and (c) show the measured results of the described experiment while Figs. 13(b) and (d) present

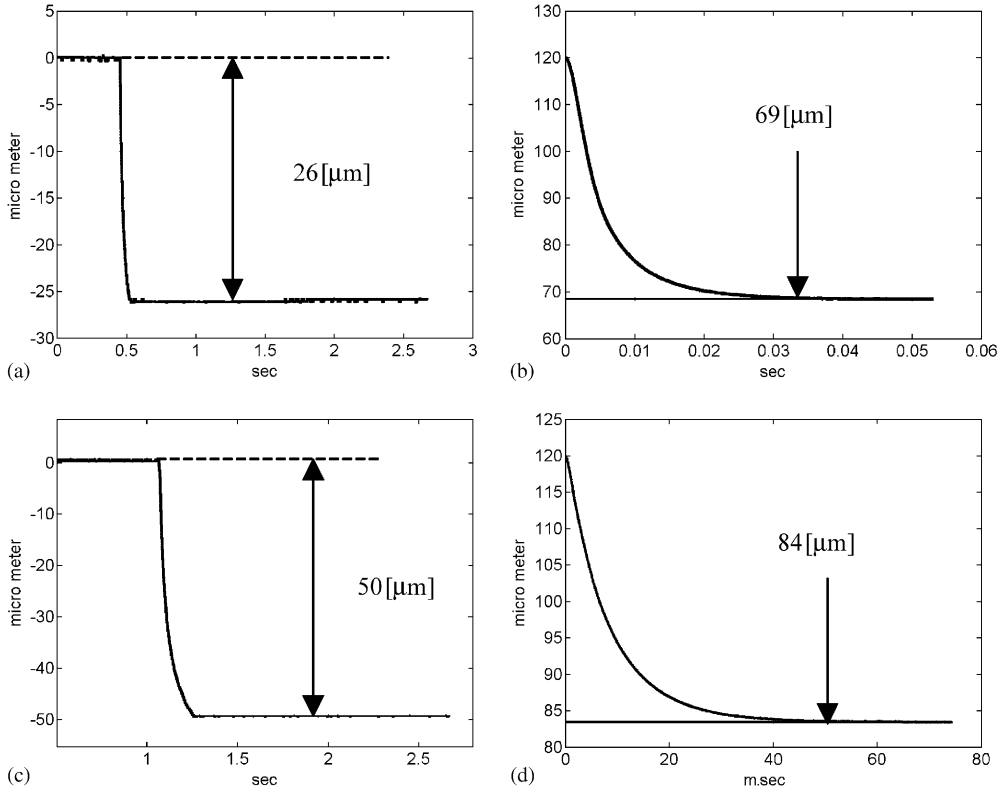

Fig. 13. Mean clearance at equilibrium between the floating disc and the transducer. Experimental results—a floating mass of: (a) 50 g, (c) 20 g. Numerical simulation—a floating mass of: (b) 50 g, (d) 20 g.

Table 3
Parameters of the numerical and experimental system

Excitation voltage (amplitude)	180 V
Excitation frequency	15 kHz
Floating mass	50, 20 g

the numerical simulation of the clearance starting form an initial gap of 120 μm. The parameters of the numerical model and the experimental model are given in Table 3.

According to the numerical simulation, equilibrium is achieved at a mean clearance of 69 μm for a mass of 50 g and 84 μm for a mass of 20 g. The experimental results show that the mean clearance is only 26 μm for a 50 g mass and 50 μm for a 20 g mass. For systems with a similar level of complexity to the one being dealt with here, there is a high probability to obtain some imperfections in the design and the manufacturing of the experimental rig. Under these constraints, the agreement that has been observed here between the numerical and experimental results is considered to be satisfactory. The simulated and measured results had a similar magnitude, and the mean clearance (in a floating state) is only about twice the measured clearance in the model. Besides the design and manufacturing limitations of the experimental model, which were discussed earlier, a possible explanation for this deviation between the results is due to the assumption that floating disc is completely rigid. In practice, the floating disc did experience some vibrations at the electrically applied frequency (see Section 3.2.3.3 below). Such vibrations absorb some of the energy conveyed by the squeeze film forces, resulting in a smaller clearance at equilibrium.

3.2.3.2. The response to external interference. Measurements for comparing the actual system's response to the external interference to the numerically simulated ones were conducted. For the sake of simplicity, we chose to create a sudden change in the weight of the floating disc by removing an added mass initially resting on the floating disc. Once equilibrium was achieved, the mass that was initially placed on the floating disc was quickly removed. The removal of a known mass can be accurately modelled numerically unlike impact forces, which require additional calibration. Such a calibration would require additional measurements at the interface between the impacting force and the floating disc, which may prove very difficult to perform. The initial floating mass was 50 g and the removed mass part was 30 g (there remaining a floating weight of 20 g).

The experimental measurements are presented in Fig. 14(a). The mass removal rate was modelled as an exponential change in the mass having that was performed with a time constant of several milliseconds. Fig. 14(b) shows the numerical simulations of the system's behaviour to such a reduction in the floating mass.

As can be observed, the system response in the numerical simulation is similar to the measured behaviour. The duration of the transient time that was observed in the simulation is in the same order of magnitude as in measured results. In the numerical simulation, the change in the mean clearance once the floating mass has been reduced is around 15 μm while the measured results indicate a difference of only 26 μm. We can observe that repeatability in the experimental

measurements as the difference in the clearance between Figs. 13(a) and (c) is 24 μm and is equal to the change in the clearance once the mass was reduced from 50 to 20 g (which is 26 μm as seen in Fig. 14(a)). Both Figs. 14(a) and (b) show that the floating mass displacement relative to the thin vibrating disc is strongly damped, reaching the equilibrium gap with almost no overshot. The low frequency vibrations appearing in the experimental measurement are caused as a result of manually removing the mass from the floating disc; therefore, removing the mass generated lateral vibrations of the floating disc. While reaching this equilibrium, the mass keeps vibrating at the excitation frequency (15 kHz) with small amplitudes relative to the clearance. This non-linear spring action of the squeeze film is related to the variations in the clearance between the discs, and is correlated to the numerical dynamic examination of the system as discussed earlier.

3.2.3.3. Vibration amplitudes of the floating disc. Finally we tried to perform a comparison between the numerical and experimental results of the vibrating amplitudes of the floating disc once it reaches the mean clearance equilibrium. In this stage, a difficulty was encountered in the comparison. The numerical algorithm assumes that the floating disc is completely stiff acting as a rigid body with no dynamic deflections. But when measuring the operating mode of the floating disc, it was discovered that the disc deforms at the frequency of excitation with a deformation pattern as shown in Fig. 15. This operating mode is asymmetric having one nodal line. If the experimental model was indeed perfectly axisymmetric, such an operating shape is not expected to

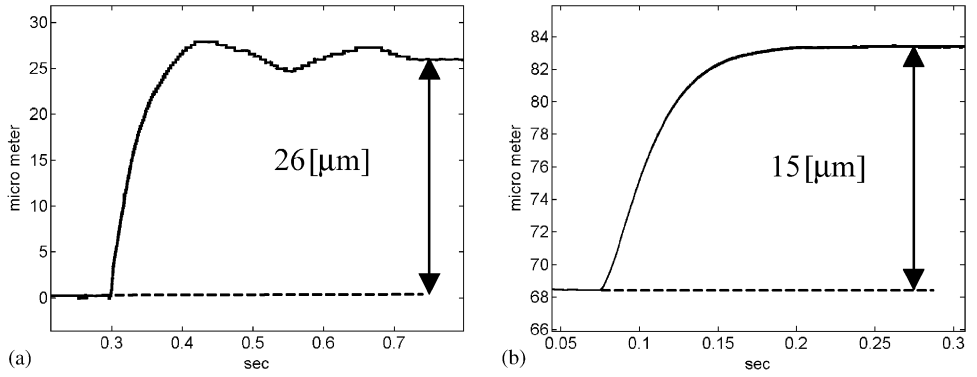

Fig. 14. Change in the mean clearance as a result of a sudden reduction of floating weight from 50 to 20 g: (a) experimental results—mean clearance change: 26 μm; (b) numerical simulation—mean clearance change: 15 μm.

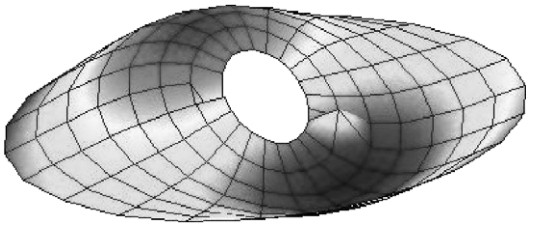

Fig. 15. Measured operating mode of the floating disc at steady state.

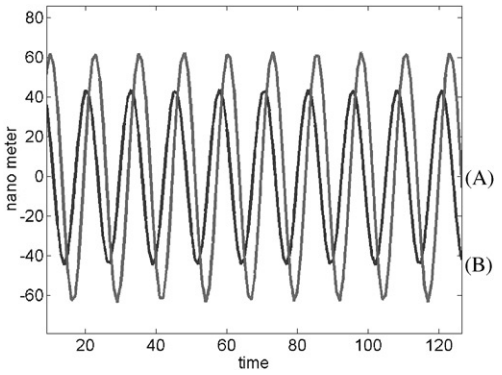

Fig. 16. Numerical simulations of the vibrating amplitudes of the floating disc at equilibrium for two different weights: (A) 20 g and (B) 30 g.

be excited. These findings emphasize the imperfections in the model and the related affects as was mentioned earlier. As the floating disc is evidently not rigid, the comparison of the amplitudes at some points on the floating disc, to the amplitudes of the floating mass in the numerical algorithm can only give a qualitative indication for the agreement. More accurate conclusions require a more elaborate numerical model.

Once equilibrium is achieved, according to the numerical simulations, as the mass of the floating disc increases, the vibration amplitudes of the floating mass at excitation frequency decrease, and vice versa. Fig. 16 shows the numerical amplitudes of two different levitated weights at equilibrium. The amplitude of a 30 g mass is near 40 nm (40×10^{-9} m) while the amplitude of a 20 g mass is near 60 nm. This behaviour was also observed in the measurements of the experimental model. Measurements on a 20 g floating disc revealed an average amplitude of 100 nm while measurements on a 30 g floating revealed average amplitudes of only 45 nm.

A better comparison between the numerical and experimental behaviour of the floating disc requires that the floating disc be modelled as a flexible structure instead of treating it as rigid body. This of course increases the level of complexity of the numerical model and consumes more calculation power. Still, under the current assumptions, the small vibration of the floating mass did not affect the average floating levels considerably (that were several orders of magnitude larger).

4. Discussion and conclusions

In conclusion, the coupled analysis contradicts earlier findings, which assume that the operating regime of the squeeze film can be divided into spring and damper regions controlled by the frequency of excitation or the squeeze number. Indeed, it is evident that the observed behaviour is more complex and has alternating regions of spring and damper that strongly depend on the mechanical structure and the combined behaviour. Different behaviour is observed for different frequencies and for different displacement scales. The numerical results emphasize the influence of the dynamic coupling effects on the individual components and the importance of these effects on the performance of the complete system.

The agreement between the numerical simulation results and the experimental measurements that have been obtained are quite satisfactory. Such an agreement has been achieved with the inclusion of the coupling effects that were considered in the numerical model. The comparable results of the numerical model and the experimental model sustain the correctness of the numerical simulation. In practice we have managed to levitate discs with a weight of over 0.5 kg, but the measurements were performed with lighter weights for convenience, as for lighter weights, the variations in clearance are larger.

The observed deviations between the numerical and experimental results' inaccuracy seem to be due to an accumulation of uncertainties in the system's behaviour, and due to some inevitable numerical-modelling assumptions. It was therefore, important to conduct a series of laboratory experiments in order to investigate the dynamical behaviour and to assess how well the numerical model represents the true behaviour. Such inaccuracies have been seen when comparing the numerical frequency response function of the electromechanical transducer to the laboratory experiments.

The mean clearance between the floating mass and the transducer was measured, indicating that the mean clearance is in the range of several tens of micrometers. The system's behaviour to an external interference was investigated, sustaining the non-linear spring action behaviour of the squeeze film and the large damping. Yet, while performing measurements on the experimental model, an unexpected behaviour was encountered that could not be revealed by the numerical model. It appears that the floating disc, in the present case, could not be assumed rigid, as we have observed an asymmetrical flexible operating mode of the disc while floating. A future investigation may focus on the combined dynamical behaviour, which incorporates a flexible floating disc.

Acknowledgements

The help of Prof. A. Yarin in the verification of the finite-difference code and the help provided by Prof. P. Bar-Yoseph with the finite element modelling are gratefully appreciated.

Appendix A. Verifying the numeric algorithm

In order to verify the solver for a non-linear problem in space and time, the compressible Reynolds equation was solved for a particular case where one expects its solution to be identical to the solution of the Blasius problem in the von Mises co-ordinates.

The latter is treated as the following:

For a two-dimensional steady flow over a plate with zero pressure gradient, the governing equations of motion in the boundary layer (the Blasius problem) are [11]

$$\frac{\partial u}{\partial x}+\frac{\partial v}{\partial y}=0,$$
$$u\frac{\partial u}{\partial x}+v\frac{\partial v}{\partial y}=v\frac{\partial^2 u}{\partial y^2} \tag{A.1}$$

with the boundary conditions

$$u(y=0)=0,$$
$$u(y=\infty)=U_\infty. \tag{A.2}$$

The stream function ψ is introduced as usual by

$$u=\frac{\partial\psi}{\partial y},\quad \upsilon=-\frac{\partial\psi}{\partial x}.$$

The von Mises transformation with the co-ordinates $\xi=x$ and $\eta=\psi$, reduce Eq. (A.1) to [11]

$$\frac{\partial u}{\partial\xi}=\frac{\partial}{\partial\psi}\left(u\frac{\partial u}{\partial\psi}\right) \tag{A.3}$$

with the boundary conditions

$$u(\psi=0)=0,$$
$$u(\psi=\infty)=U_\infty=1\quad (U_\infty=1\ \text{and}\ v=1\ \text{for simplicity}). \tag{A.4}$$

It is well known that the Blasius problem has a self-similar solution

$$\psi=\sqrt{x}f(\eta),$$
$$u=f'(\eta), \tag{A.5}$$

where $\eta=y/\sqrt{x}$ and the functions f, f' are tabulated in Ref. [11].

This solution can be presented with the von Mises transformation as $u=F(\psi/\sqrt{\xi})$. Problem (A.3) and (A.4) is a particular hypothetical case of the compressible Reynolds equation in Cartesian co-ordinates for a constant uniform gap. Therefore, for the sake of comparison, one could treat u in Eqs. (A.3) and (A.4) as the pressure P in the Reynold's equation. Self-similarity

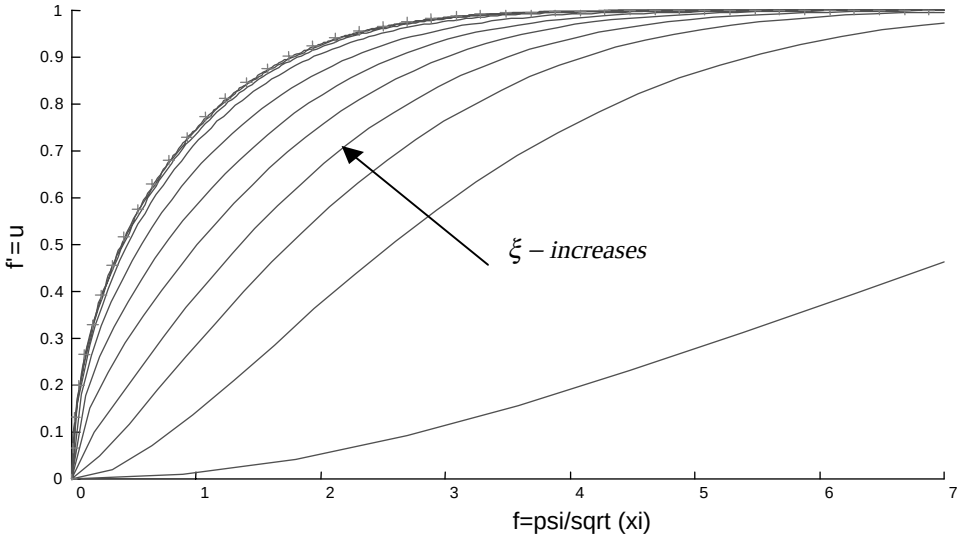

Fig. A.1. Numerical simulating results for several particular values of ξ.

means that a solution of problem (A.3) with any arbitrary "initial" condition, which satisfies the boundary conditions, such as

$$u(\xi = 0) = 1 - e^{-\psi^2} \tag{A.6}$$

should converge to the self-similar form $u = F(\psi/\sqrt{\xi})$ as $\xi \to \infty$ and moreover, the function F could be reconstructed from Blasius solution by $f' = F(f)$.

The results of the numerical simulating, using the code, are plotted in Fig. A.1 for several particular values of ξ. It is clearly seen that the curves converge to a limiting curve beginning from $\xi = 0.0124\ldots\xi^*$, and this curve (marked by crosses) is indeed identical to the results of Blasius problem.

It is obvious that a similar convergence should be achieved for any other initial condition replacing that of Eq. (A.6); only the "convergence time" ξ^* would change. The Blasius solution is regarding a boundary layer away from the front edge of the plate, where the edge effects do not influence the flow profile. This explains why the numeric solution converges as ξ increases. Imposing the arbitrary initial condition actually describes the flow profile on the plate's front edge.

Appendix B. Finite elements verification

Verification of the finite elements algorithm for an axisymmetric piezoelectric structure was made by comparing to the results obtained by Guo et al. [2] and the results obtained by Heyliger et al. [10] for a piezoelectric disc made of PZT-5A with polarization in the axial direction and the electrodes are on the upper and lower bases of the disc. The natural frequencies were found by solving the eigenvalue problem for the short-circuit case given by Eq. (12). The disc's dimensions are 19.96 mm in diameter and 2.01 mm in thickness. In the work by Gou et al. [3] and that by Heyliger and Ramirez [10], a 2×48 mesh of eight-node quadrilateral axisymmetric piezoelectric elements was used. In this work, the piezoelectric disc has been modelled by four-node quadrilateral axisymmetric piezoelectric elements. Therefore a mesh of 4×96 has been used. Finer meshes were also used, and it was found that the accuracy was not significantly improved while the cost of computing increased drastically.

There is an excellent agreement between the results as can be seen in Table B.1 which shows a comparison between the results obtained by Gau et al. [3], Heyliger and Ramiren [10] and this work for the first five symmetric modes frequencies.

Table B.1
Symmetric mode frequencies (kHz) of traction-free PZT-5A disc

Mode	Guo [6]	Heyliger [7]	F.E.M.	Rel Diff Guo (%)	Rel Diff Heyliger (%)
1	99.21	99.22	99.2135	0.0035	−0.0066
2	252.4	252.38	252.4801	0.0317	0.0397
3	384.8	383.88	385.1991	0.1037	0.3436
4	493.2	497.38	494.4846	0.2605	−0.5821
5	572.2	577.59	578.1011	1.0313	0.0884

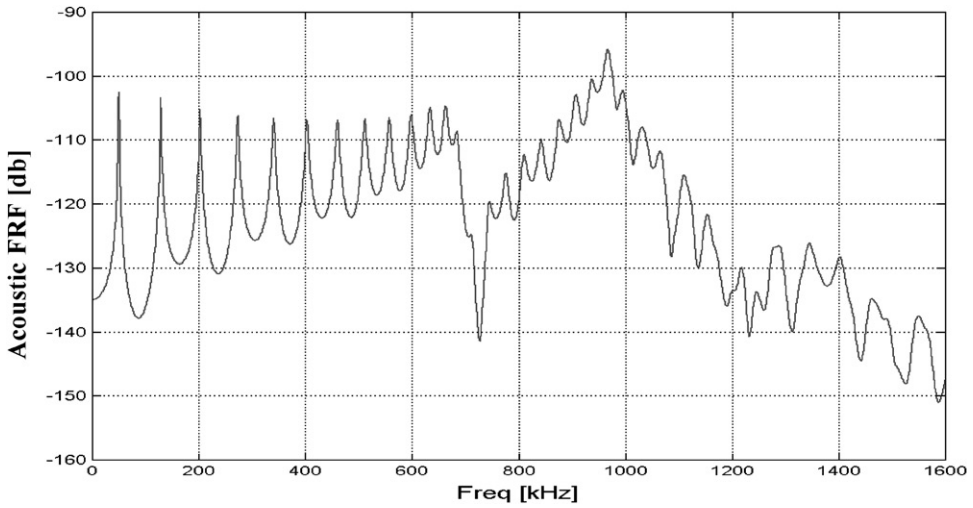

Fig. B.1. Frequency response function of the centre point of the piezoelectric disc derived by Mode superposition analysis with 0.013 damping factor.

The mechanical frequency response functions in the axial direction of the centre of the surface when voltage excitation is applied, is shown in Fig. B.1. Structural damping, which is proportional to the stiffness, of a factor of 0.013 was introduced in the frequency response function. At relatively low frequencies, there is an excellent agreement, which is slowly deteriorating as the frequency increases. The accuracy of the FRF is determined by the number of modes taken into consideration in the mode superposition method. The peaks seen in Fig. B.1 are at resonance frequencies of the extensional mechanical modes as explained in Section 2.3.1.

Appendix C. Numerical assembly of the transducer sub-components

A useful and convenient way to model a complex system is by sub-dividing the system into a group of smaller and simpler problems, solving each problem separately and then regrouping the system's components under the appropriate constrains. Such an approach is made possible by a transformation, which allows only motions that do not perform any work on the immovable constraints. In this work, this transformation was performed in order to combine the stack of piezoelectric discs together with the exponential horn and the thin disc. The advantage of such an assembly is the ability to mesh relatively simple geometries separately. As the meshing has a significant effect on the convergence and accuracy of the finite elements model, such ability is important.

Let $\mathbf{q}_A$, $\mathbf{q}_B$ be the vectors containing the d.o.f. of parts A and B, respectively. The interface d.o.f., which are the d.o.f. sheared by both parts, are subsets of vectors $\mathbf{q}_A$, $\mathbf{q}_B$. Therefore one can write the interface d.o.f. $\mathbf{q}_1$, $\mathbf{q}_2$ as

$$\mathbf{q}_1 = [\mathbf{S}_1]\{\mathbf{q}_a\}, \quad \mathbf{q}_2 = [\mathbf{S}_2]\{\mathbf{q}_b\}, \tag{C.1}$$

where

$$\mathbf{S}_i = \begin{bmatrix} 0 & 1 & 0 & \dots \\ 0 & 0 & 1 & \dots \\ \vdots & \vdots & \vdots & \ddots \end{bmatrix}$$

are selection matrices extracting the desired d.o.f. from the total vector of d.o.f.

By designating $\mathbf{Q}_1, \mathbf{Q}_2$ as the forces acting on the interface between parts A and B, and by assigning $\mathbf{Q}_A$, $\mathbf{Q}_B$ as the total forces (not including the interface forces) acting on parts A and B, respectively, the total virtual work done on the two parts may be written as

$$\delta W = \mathbf{Q}_a \delta \mathbf{q}_a + \mathbf{Q}_b \delta \mathbf{q}_b + \mathbf{Q}_1 \delta \mathbf{q}_1 + Q_2 \delta \mathbf{q}_2. \tag{C.2}$$

By definition, the sum of the virtual work done by the interface forces is zero; therefore $\mathbf{Q}_1 \delta \mathbf{q}_1 + \mathbf{Q}_2 \delta \mathbf{q}_2 = \mathbf{0}$. Making use of Newton's third law, one gets

$$[\mathbf{S}_1, -\mathbf{S}_2] \begin{Bmatrix} \delta \mathbf{q}_a \\ \delta \mathbf{q}_b \end{Bmatrix} = 0. \tag{C.3}$$

This expression indicates that any virtual displacements of the general d.o.f. (not including the interface d.o.f.) are in space spanned by the kernel of the matrix $[\mathbf{S}_1, \quad -\mathbf{S}_2]$. The uncoupled dynamic equations of the parts A and B may be written in a matrix form as

$$\begin{bmatrix} \mathbf{M}_a & \mathbf{0} \\ \mathbf{0} & \mathbf{M}_b \end{bmatrix} \begin{Bmatrix} \ddot{\mathbf{q}}_a \\ \ddot{\mathbf{q}}_b \end{Bmatrix} + \begin{bmatrix} \mathbf{C}_a & \mathbf{0} \\ \mathbf{0} & \mathbf{C}_b \end{bmatrix} \begin{Bmatrix} \dot{\mathbf{q}}_a \\ \dot{\mathbf{q}}_b \end{Bmatrix} \begin{bmatrix} \mathbf{K}_a & \mathbf{0} \\ \mathbf{0} & \mathbf{K}_b \end{bmatrix} \begin{Bmatrix} \mathbf{q}_a \\ \mathbf{q}_b \end{Bmatrix} = \begin{Bmatrix} \mathbf{Q}_a \\ \mathbf{Q}_b \end{Bmatrix}, \tag{C.4}$$

where $\mathbf{M}$, $\mathbf{C}$, $\mathbf{K}$ are the mass, damping, and stiffness matrices, respectively.

Applying the transformation

$$\begin{Bmatrix} \mathbf{q}_a \\ \mathbf{q}_b \end{Bmatrix} = [\mathbf{T}]\{\mathbf{a}\}$$

where $[\mathbf{T}] = Span(Ker[\mathbf{S}_1, \quad -\mathbf{S}_2])$ is the subspace generated (spanned) by the vectors forming the null space (kernel) of the matrix $[\mathbf{S}_1, \quad -\mathbf{S}_2]$ and $\{\mathbf{a}\}$ is a generalized co-ordinates vector; together with pre-multiplying by $[\mathbf{T}]^{\mathrm{T}}$, the uncoupled dynamic equations are transformed to a set of coupled equation:

$$[\bar{\mathbf{M}}]\{\ddot{\mathbf{a}}\} + [\bar{\mathbf{C}}]\{\dot{\mathbf{a}}\} + [\bar{\mathbf{K}}]\{\mathbf{a}\} = [\mathbf{T}]^{\mathrm{T}} \begin{Bmatrix} \mathbf{Q}_a \\ \mathbf{Q}_b \end{Bmatrix}, \tag{C.5}$$

where $[\bar{\mathbf{M}}]$, $[\bar{\mathbf{C}}]$, $[\bar{\mathbf{K}}]$ are the mass, damping, and stiffness matrices after transformation , respectively.

Solving the transformed Eq. (C.5) and reversing the transformation, produces the d.o.f. solutions for each separated part under the bounding constraints.

References

[1] E.O.J. Salbu, Compressible squeeze films and squeeze bearings, Journal of Basic Engineering 86 (1964) 355–366.
[2] W. Wiesendanger, U. Probst, R. Siegwart, Squeeze film air bearings using piezoelectric bending elements, Proceedings of the Fifth International Conference on Motion and Vibration Control (MOVIC2000), Sydney, Australia, 2000, pp. 181–186.
[3] N. Guo, P. Cawley, D. Hitchings, The finite element analysis of the vibration characteristics of piezoelectric discs, Journal of Sound and Vibration 159 (1992) 115–138.
[4] Y. Kagawa, T. Yamabuchi, Finite elements approach for a piezoelectric circular rod, IEEE Transactions on Sonics and Ultrasonics SU-23 (6) (1976) 379–385.
[5] IEEE Standard on Piezoelectricity—Std. 176, The Institute of Electrical and Electronics Engineering, New York, 1987.
[6] H.F. Tiersten, Linear Piezoelectric Plate Vibrations, Plenum Press, New York, 1969.
[7] M. Naillon, R.H. Coursant, F. Besnier, Analysis of piezoelectric structures by finite elements method, Acta Electronica 25 (4) (1983) 341–362.
[8] W.E. Langlois, Isothermal squeeze films, Quarterly of Applied Mathematics XX (2) (1962) 131–150.
[9] W.P. Mason, Electromechanical Transducers and Wave Filters, Princeton University Press, Princeton, NJ, 1948.
[10] P.R. Heyliger, G. Ramirez, Free vibrations of laminated circular piezoelectric plates and discs, Journal of Sound and Vibration 229 (4) (2000) 935–956.
[11] H. Schlichting, Boundary-Layer Theory, McGraw-Hill, New York, 1979.